

## Numerical Analysis of Reinforced Embankment Over Soft Foundation

Javad Safadoust<sup>1</sup>, Shahin Nayyeri Amiri<sup>2</sup> and Asad Esmacily<sup>2</sup>

<sup>1</sup> Department of Civil Engineering, Tabriz University, Iran,

<sup>2</sup> Department of Civil Engineering, Kansas State University, Manhattan, KS 66506, USA

Received 21 July 2013; Accepted 10 December 2013

### Abstract

This paper describes a finite element analysis of geosynthetic reinforced embankment constructed on soft cohesive foundation under partially drained condition. The behaviour of embankment and foundation soils were simulated using the hyperbolic hardening soil model and soft soil model, respectively. In order to investigate the effect of surcharge on the embankment behaviour, a uniformly-distributed loading was considered as a surcharge after the end of construction. Construction and loading sequence and consolidation were modelled. The effects of the reinforcement stiffness on the horizontal and vertical displacements, mobilized reinforcement force and embankment failure surcharge were considered. The effect of loading rate on the embankment failure surcharge was also evaluated. It was shown that reinforcement can significantly reduce the maximum lateral deformation and increase the embankment failure surcharge.

*Keywords:* reinforced embankment; soft soil; finite element analysis.

### 1. Introduction

Geosynthetics are often used to improve performance of embankments over soft foundation soils. Traditional soil improvement methods include preloading/surcharging with drains; lightweight fill; excavation and replacement; embankment piles and etc. In some situations geosynthetic reinforcement may be the most economical design in comparison to the traditional methods. Reinforced embankments can be studied using various methods, including finite element modelling, limit equilibrium methods, serviceability based design methods, centrifuge modelling and field trials. The finite element technique is well recognized as powerful analysis and design tool and, many example of its application to the analysis and the design of reinforced embankments can be found in the literature. Methods of analysis such as limit equilibrium method provide no information about deformations or strains, which develop in the reinforcement for a given reinforced embankment. The cost of constructing and monitoring full-scale field test embankments is sufficiently large that it is generally impractical.

Bassat and Yeo[1] described the construction of a geogrid reinforced embankment over a deep soft clay deposits at Stanstead Abbots, U.K. Several inclinometers, hydraulic, pneumatic piezometers, horizontal profile gauge, load cells and strain measuring devices were used at this trial embankment. The magnitude of maximum tensile force in the geogrids was 16kN/m. The results of the geotechnical instrumentation, testing and monitoring of a fabric reinforced dyke at New Bedford harbour, U.S.A. were presented by Fowler et al. [2]. The maximum horizontal movement observed in the inclinometers was 7.6 cm and

total downward displacement of the settlement plates was in the 0.9m to 1.2m range. Maximum strain in the fabric was 5.5-7% at the end of construction. Chai et al. [3] described a case history of both reinforced and unreinforced embankments built to failure on soft subsoil at Lian-Yun-Gang, China. The foundation soil consisted of a 2.0 m thick clay crust underlain by 8.5 m thick soft clay layer. Sandy clay was used as a fill material. The reinforcement material used was in the range of 800-1600kN/m. The unreinforced embankment failed at a fill thickness of 4.04m, while the reinforced embankment failed at a fill thickness of 4.35m.

Rowe and Soderman [4] used the finite element model to examine a geotextile reinforced embankment constructed on peat, underlain by a firm base. The stabilizing effect of the geotextile was shown to increase with the increase in geotextile modulus and the effect was more significant for shallower deposits. Hinchberger and Rowe [5] studied stages 1 and 2 of the Gloucester test embankment using a fully coupled finite element model. The elliptical cap model was used for the time-dependant plastic foundation soil. The measured and calculated settlements were generally in good agreement for the two stages of Gloucester test embankment construction. Varadarajan et al. [6] conducted a parametric study of a reinforced embankment using coupled elastoplastic finite element analysis. For smaller foundation depth, they noted that the effect of reinforcement stiffness was enhanced, as was the force in the reinforcement and the height of the embankment. The effectiveness of reinforcement with high stiffness was shown to depend on the magnitude of shear strength of clay-reinforcement interface.

The objective of this paper is to provide insight regarding the behaviour of reinforced embankments over soft foundation by using the finite element analysis. The factors considered include the elastic-plastic properties of the foundation soil, the non-linear elastic behaviour of the

\* E-mail address: tabunjs@yahoo.com

fill, reinforcement stiffness, and the construction and uniform surcharge rates.

## 2. Finite Element Analysis

### 2.1. General procedures

In this study, the construction of a reinforced embankment in Tehran-Shomal highway in Iran (see Fig. 1) with 21m crest width and 2(horizontal):1(vertical) side slopes was examined. The soft foundation was 8m deep and underlain by a relatively permeable layer. The water table was at the depth of 2.5m and the initial pore pressures prior to embankment construction were taken to be hydrostatic. A uniform-distributed surcharge was considered for modelling the traffic load and investigating the effect of surcharge on the reinforced embankment. The finite element analysis of the embankment described above was conducted using PLAXIS. The embankment was simulated as a plane-strain, two dimensional problems for the finite element analysis. The soil was simulated using 15-node triangular elements. The geotextile was simulated using 5-node geotextile element with a normal stiffness but with no bending stiffness. Geotextile element can only sustain tensile forces and no compression. For this study, reinforcement material was modelled as linear elastic elements. The elastic-plastic interface elements were used to simulate the soil/geotextile interaction. Interface elements were connected to soil elements and an elastic-plastic model was used to describe the behaviour of interface elements. To eliminate possible boundary effects, the foundation soil was extended to a distance of 60m in the front end. The side boundaries were rollers whereas the base was fixed. Fig. 2 shows the soil mesh used for the analysis. The mesh consists of 369 soil elements, 9 geotextile elements and 18 interface elements. Embankment construction was simulated by placing 0.4m thick lifts such that the body forces were applied using 100 incremental load steps. The construction rate of 0.5m/month and the loading rate of 18.18kN/m<sup>2</sup>/month were used and the upper and lower surfaces of the clay layers were assumed to be free draining boundaries. The compaction effects were not considered in this study since it is difficult to determine the initial states of soil prior to compaction. Moreover, the compaction effects are usually erased by the overburden stresses toward the end of construction as indicated by seed [7].

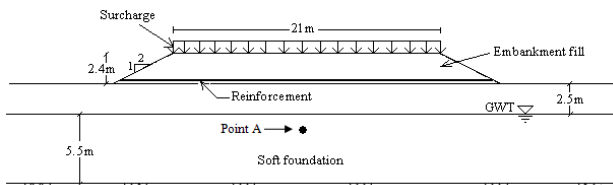


Fig. 1. Reinforced Embankment and Foundation.

### 2.2. Embankment soil

The embankment fill was a bad graded sand with a friction angle  $\phi = 41^\circ$ , dilatancy angle  $\psi = 8^\circ$ , and a unit weight  $\gamma = 20\text{kN/m}^3$ . The Hardening-Soil model was used to simulate embankment fill behaviour. The Hardening-Soil model is an advanced model for simulating the behaviour of different types of soil

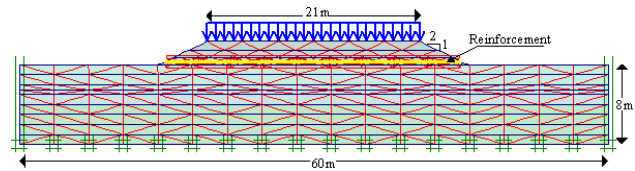


Fig. 2. FEM Mesh

(Schanz [8]). In this model, the relationship between the axial strain and the deviatoric stress can be well approximated by a hyperbola as shown in Eq.(1).

$$-\varepsilon_1 = \frac{1}{2E_{50}} \frac{q}{1 - \frac{q}{q_{ult}}} \quad \text{for: } q < q_f \quad (1)$$

Where  $q_{ult}$  is the ultimate deviatoric stress,  $q_f$  is the deviatoric stress at failure and  $E_{50}$  is the secant modulus at 50% strength as shown in Fig. 3. Such a relationship was first formulated by Kondner [9] and later used in the well-known hyperbolic model (Duncan & Chang, [10]). The parameter  $E_{50}$  can be given by the Eq. (2).

$$E_{50} = E_{50}^{ref} \left( \frac{c \cos \varphi - \sigma'_3 \sin \varphi}{c \cos \varphi + p^{ref} \sin \varphi} \right)^m \quad \sigma'_3 \text{ is}$$

negative for compression (2)

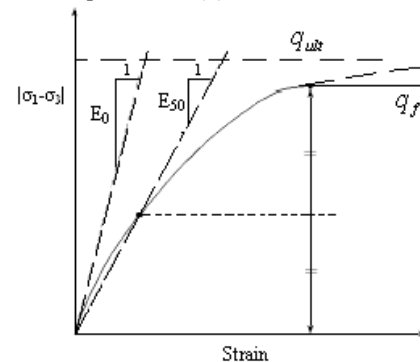


Fig. 3. Definition of E0 and E50.

Where  $E_{50}^{ref}$  is a reference stiffness modulus corresponding to the reference confining pressure  $p^{ref}$ . In Plaxis, a default setting  $p^{ref} = 100$  stress units is used. The actual stiffness depends on the minor principal stress,  $\sigma'_3$ , which is the confining pressure in the triaxial test. Deviatoric stress at failure,  $q_f$ , and the ultimate deviatoric stress  $q_{ult}$  in Eq.(1) are defined as:

$$q_f = (c \cot \varphi - \sigma'_3) \frac{2 \sin \varphi}{1 - \sin \varphi} \quad (3)$$

$$q_{ult} = \frac{q_f}{R_f} \quad \text{and } R_f < 1 \quad (4)$$

The above relationship for  $q_f$  is derived from the Mohr-Coulomb failure criterion. As soon as  $q = q_f$ , the failure criterion is satisfied and perfectly plastic yielding occurs.

Four triaxial tests ( $\sigma'_3 = 60\text{kN/m}^2, 100\text{kN/m}^2, 300\text{kN/m}^2$  and  $500\text{kN/m}^2$ ) were used to obtain the hyperbolic model

parameters  $E_{50}^{ref}$  and  $m$ . For this purpose the secant modulus,  $E_{50}$ , and the ultimate deviatoric stress,  $q_{ult}$ , for each triaxial test were first determined. These parameters were determined by plotting axial strain versus deviator stress. The parameters  $E_{50}^{ref}$  and  $m$  can be determined by plotting  $E_{50}$  versus  $\sigma_3'/p^{ref}$  on a log-log scale. The best-fit straight line was drawn in Fig. 4. From Fig. 4 values of  $m$  and  $E_{50}^{ref}$  are 0.57 and 27770kN/m<sup>2</sup>, respectively. Soil/reinforcement interface friction angle was equal to 35.2°.

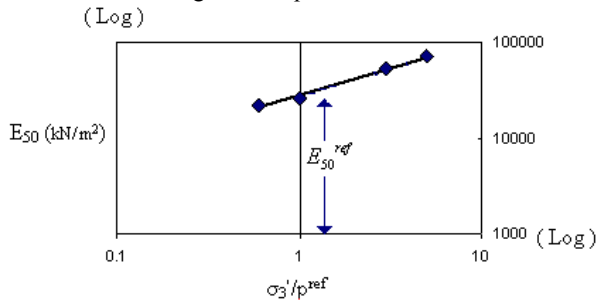


Fig. 4. Determination of  $m$  and  $E_{50}^{ref}$ .

**2.3. Foundation soil**

The soft clay had a liquid limit of 71% and a plasticity index of 37%. The preconsolidation pressure,  $\sigma_p'$ , profile was shown in Fig. 5. The initial void ratio and unit weight of the clay deposit at ground surface were 1.7 and 16 kN/m<sup>3</sup>. The variation in unit weight and void ratio with depth were taken to be consistent with the initial void ratio and unit weight at the ground surface, the preconsolidation pressure profile and the compression and recompression indices.

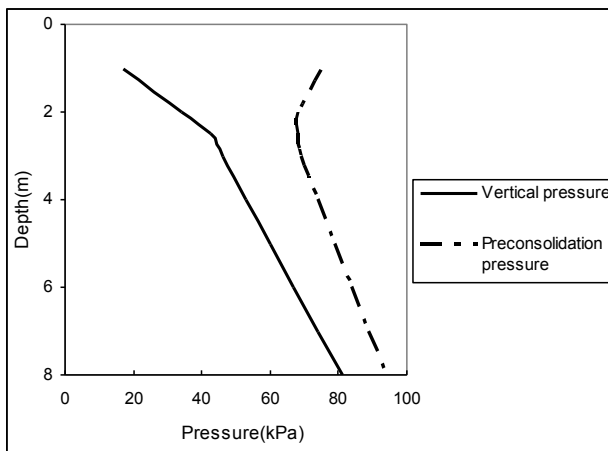


Fig. 5. Preconsolidation Profile of Foundation Soil.

The soil above the water table was taken to be saturated but, the capillary action was not taken into account for determining the effective soil stress. The Soft-Soil model was used to simulate embankment fill behaviour. In the Soft-Soil model, it is assumed that there is a logarithmic relation between the volumetric strain,  $\epsilon_v$ , and the mean effective stress,  $p'$ , which can be formulated as:

$$\epsilon_v - \epsilon_v^0 = -\lambda^* \ln\left(\frac{p'}{p^0}\right) \quad (\text{virgin compression}) \quad (5)$$

$$\epsilon_v^e - \epsilon_v^{e0} = -\kappa^* \ln\left(\frac{p'}{p^0}\right) \quad (\text{unloading and reloading}) \quad (6)$$

$$\kappa^* = \kappa / (1+e) \quad (7)$$

$$\lambda^* = \lambda / (1+e) \quad (8)$$

The Soft-Soil model defines the compression yield function for  $\sigma_2' = \sigma_3'$  as:

$$f = \bar{f} - p_p \quad (9)$$

$$\bar{f} = \frac{q^2}{M^2(p' + c \cos \varphi)} + p' \quad (10)$$

$$p_p = p_p^0 \exp\left(\frac{-\epsilon_v^p}{\lambda^* - \kappa^*}\right) \quad (11)$$

Where  $\epsilon_v^p$  is the volumetric plastic strain and  $p_p^0$  is the initial value of the pre-consolidation stress. The yield function  $\bar{f}$  describes an ellipse in the  $p'$ - $q$  plane as illustrated in Fig. 6. The parameter  $M$  determines the height of the ellipse. To model the failure state, a perfectly-plastic Mohr-Coulomb type yield function was used as shown in Fig. 6. For general states of stress, the plastic behaviour of the Soft-Soil model is defined by a total of six yield functions; three compression yield functions and three Mohr-Coulomb yield functions. The foundation soil parameters are summarized in Table 1.

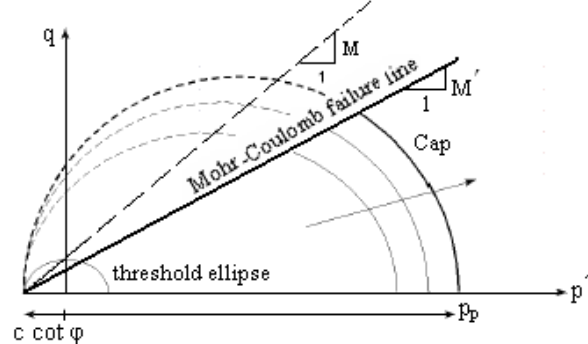


Fig. 6. Yield Surface of the Soft-Soil Model in  $p'$ - $q$  Plane.

**Table 1.** Soft-Soil model parameters.

Friction angle	28°
Cohesion	0
Compression index $\lambda^*$	0.067
Recompression index $\kappa^*$	0.011
Void ratio at ground surface $e_0$	1.7
$M$	1.514
$M'$	1.117
Horizontal hydraulic conductivity $k_{v0}$	0.0004m/day
$k_h / k_v$	3

**2.3. Interface properties and reinforcement stiffness**

In Plaxis, the interface properties were calculated from the soil properties by applying the following rules:

$$c_i = R_{inter} c_{soil} \quad (12)$$

$$\tan \phi_i = R_{inter} \phi_{soil} \quad (13)$$

$$\psi_i = 0^\circ \text{ for } R_{inter} < 1, \text{ otherwise } \psi_i = \psi_{soil} \quad (14)$$

$$G_i = R_{inter}^2 G_{soil} \quad (15)$$

$$\nu_i = 0.45 \quad (16)$$

Where  $R_{inter}$  is the strength reduction factor for interfaces. Reinforcement with tensile stiffness, J, varying from 0 (no reinforcement) to 8000kN/m was examined.

### 3. Result and Discussion

#### 3.1. Excess pore water pressure

Fig. 7-a shows the contour of excess pore water pressure beneath the embankment at the end of construction. It can be seen that the maximum excess pore water pressure occurred at the center line beneath the embankment and at a distance of about 4m from the ground surface. Fig. 7-b shows the excess pore water pressure at point A located at the center line beneath the embankment and at a distance of 4m from the ground surface during the construction and surcharge loading up to 100kN/m<sup>2</sup> for the unreinforced position.

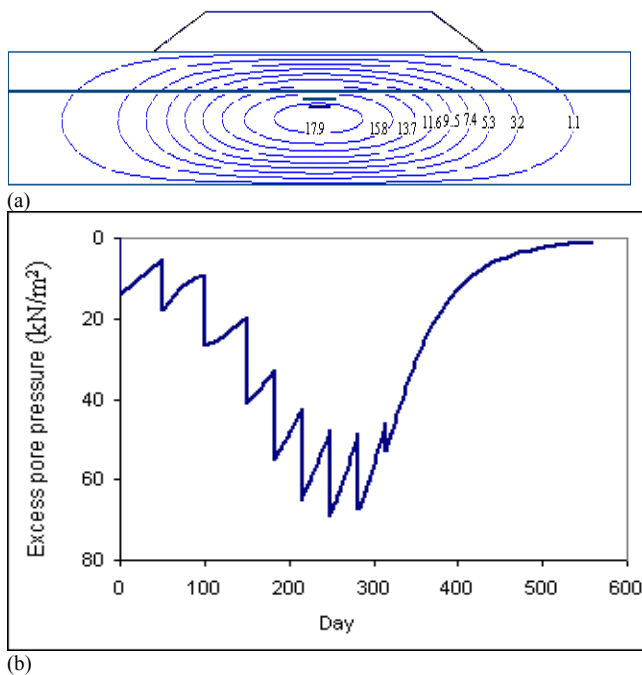


Fig. 7. (a) Excess pore Water Pressure Beneath the Embankment at the End of Construction (b) Excess Pore Water Pressure at Point A.

#### 3.2. Failure surcharge of embankment

Fig. 8 shows the calculated embankment failure surcharge. The unreinforced embankment failure surcharge was 107 kN/m<sup>2</sup>. A change of reinforcement stiffness up to 8000 kN/m resulted in an increase in failure surcharge by 107 kN/m<sup>2</sup> relative to the unreinforced case. The increase in reinforcement stiffness had a significant effect on the embankment failure surcharge up to J=2000 kN/m. For J greater than 4000 kN/m, the increase in the reinforcement stiffness no longer influenced the failure surcharge.

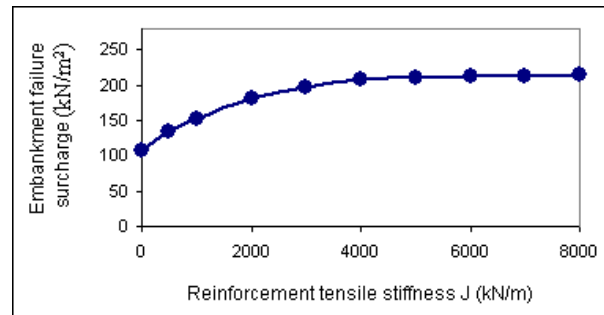


Fig. 8. Embankment Failure Surcharge vs. Reinforcement Tensile Stiffness.

#### 3.3. Horizontal and vertical displacement

Fig. 9 shows the horizontal displacement at the toe of the embankment. As shown in Fig. 9 the effect of reinforcement was more significant for greater surcharge. A change of reinforcement stiffness from 500 kN/m to 8000 kN/m resulted in a decrease in horizontal displacement by between 25% to 41%. Fig. 10 shows the distribution of the vertical displacement along the ground surface. As shown in Fig. 10 The maximum vertical displacement decreased by about 8.5 % and 9 % respectively for surcharge = 60 kN/m<sup>2</sup> and 120 kN/m<sup>2</sup> when the reinforcement modulus increased from 0 to 8000 kN/m. Comparing the effect of the reinforcement on the vertical and horizontal displacement with together showed that the inclusion of reinforcement had significant effect in reducing the horizontal displacement.

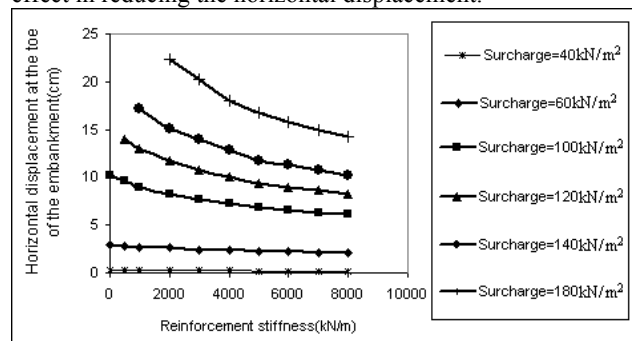


Fig. 9. The Variation of Maximum Horizontal Displacement With Reinforcement Stiffness and Surcharge.

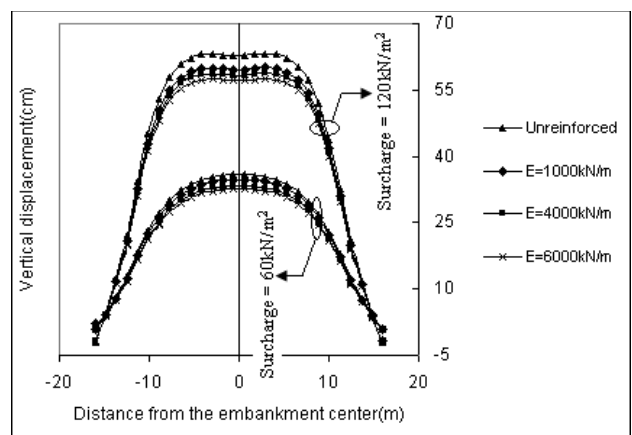


Fig. 10. The Variation of Maximum Vertical Displacement With Reinforcement Stiffness and Surcharge.

#### 3.4. Reinforcement strain

Fig. 11-a shows the calculated failure strain in the reinforcement. As shown in Fig. 11-a the calculated

maximum reinforcement failure strain is related to  $J = 2000$  kN/m. Fig. 11-b shows the reinforcement strain during construction and surcharge loading. As shown in Fig. 11-b the rate of reinforcement strain changed sharply when the embankment loading became higher than  $40\text{kN/m}^2$ . Fig. 11 shows that the maximum reinforcement strain was about 2.5% and consequently, the mobilized reinforcement tensile force would be relatively small. This shows that why the observed field strains were typically so low. The Almere test embankment (Rowe [11]) reinforced by one layer of geotextile yielded a strain of approximately 2.5% at a critical height of 2.05 m. The Sackville embankment (Rowe et al. [12]), using woven geotextile having a secant stiffness of  $1466$  kN/m at 5% strain, showed that the measured maximum strain corresponding to the primary failure at a 5.7 m fill thickness was approximately 3%. Also, the critical strain of approximately 3% was found for the case of the Guiche test embankment (Delmas et al. [13]) in which one layer of geotextile having a tensile stiffness of  $2250$  kN/m was used as reinforcement. Li and Rowe [14] showed that the magnitude of reinforcement strain at working conditions typically ranges between 1% and 3% using the finite element analysis. Fig. 12 also shows relationships between the reinforcement stiffness and the mobilized reinforcement force for various surcharges. As shown in Fig. 12 there were approximately two separate linear relationships between the reinforcement stiffness and the mobilized reinforcement force for  $J < 2000$  kN/m and  $J > 2000$  kN/m. From Fig.12 for a certain value of surcharge, the following relations can approximately be derived.

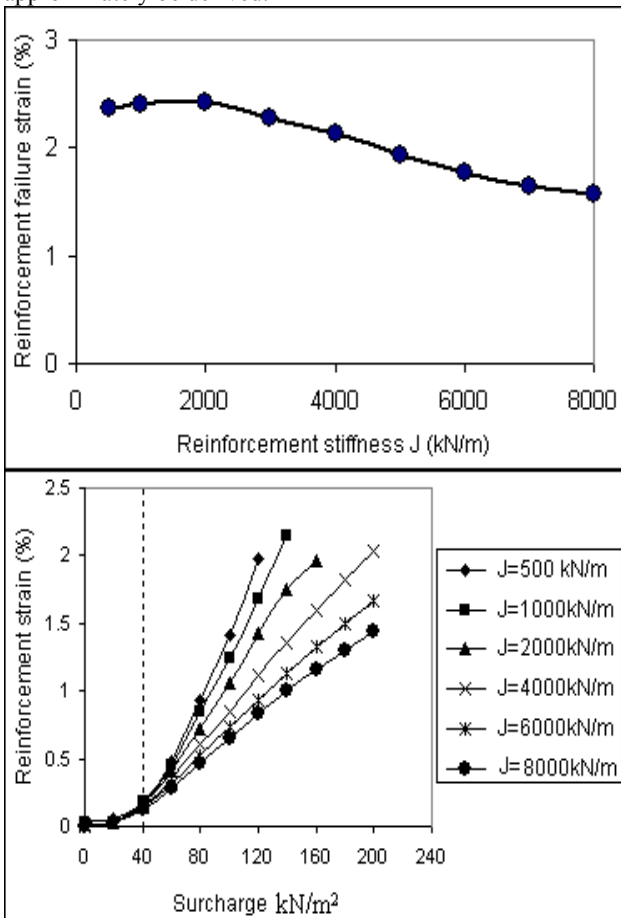


Fig. 11. (a) Reinforcement Strain at Failure Surcharge, (b) Variation of Reinforcement Strain With Reinforcement Stiffness and Surcharge Loading.

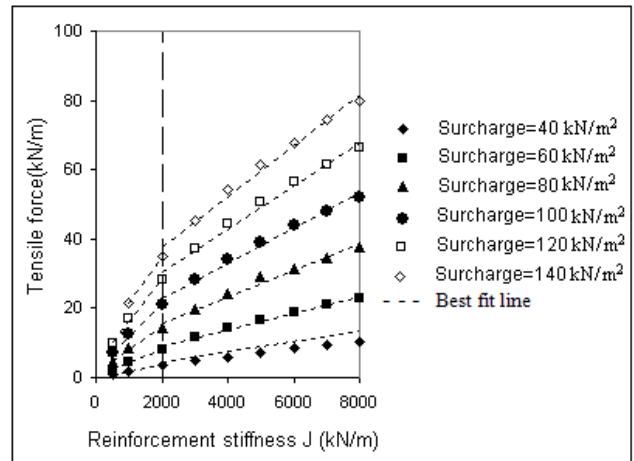


Fig. 12. Relationships Between the Reinforcement Stiffness and the Mobilized Reinforcement Force.

$$\frac{F_2 - F_1}{J_2 - J_1} = \alpha \quad J_{1,2} > 2000 \text{ kN/m} \quad (17)$$

$$\frac{F_2 - F_1}{J_2 - J_1} = \beta \quad J_{1,2} < 2000 \text{ kN/m} \quad (18)$$

Where:

$\alpha$  and  $\beta = \text{constant}$

$F_1$  and  $F_2 = \text{maximum mobilized reinforcement force corresponding to the reinforcement stiffness } J_1 \text{ and } J_2.$

### 3.5. Tensile force and tangential shear stress distribution of reinforcement

The main target of reinforcement is to inhibit the development of stresses in the soil and to support the tensile stresses that the soil can not withstand. The tensile force supported by geogrid improves the soil mechanical properties by reducing the shear stress that has to be carried by the soil and by increasing its available shearing resistance. Tensile force, tangential shear stress and horizontal displacement distributions of reinforcement at failure surcharge (see Fig. 8) were shown in Fig. 13 for  $J = 1000$  kN/m,  $J = 3000$  kN/m and  $J = 5000$  kN/m. As shown in Fig. 13 the maximum tensile force occurs at a lateral distance of about 9m to 10m from the center of the embankment.

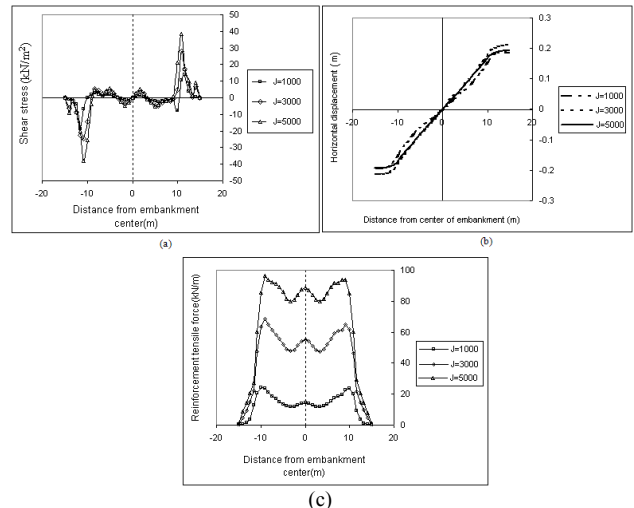


**Fig. 13.** Distributions of (a) Tangential Shear Stress,(b) Horizontal Displacement and (c) Tensile Force in the Reinforcement at Failure Surcharge.

Fig. 14 shows the differential soil and reinforcement elements. For the condition given in Fig.14 the following equilibrium equations can be derived.

$$\tau(x) = \tau_t(x) + \tau_b(x) \tag{19}$$

$$\frac{dF(x)}{dx} = -\tau(x) \tag{20}$$

$$\varepsilon(x) = \frac{du(x)}{dx} \tag{21}$$

$$\frac{du(x)}{dx} = \frac{F(x)}{J} \tag{22}$$

Where:

- J = modulus of the reinforcement.
- u(x) = horizontal displacement in the reinforcement (positive in the x direction).
- F(x) = tensile force in the reinforcement.
- $\tau(x)$  = tangential shear stress in the reinforcement.
- $\varepsilon(x)$  = strain in the reinforcement.

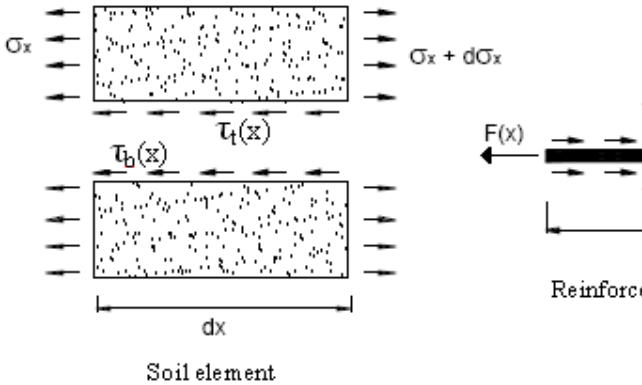


**Fig. 14.** Equilibrium of Differential Soil and Reinforcement Elements.

As shown in Fig. 13-a there are several sections in the reinforcement which their tangential shear stress is equal to zero. According to the Eq. (19), this means that the tangential shear stress on the upper face of the reinforcement is equal to the negative of that on its lower face.

With the extension of Eqs. (17) and (18) to the mobilized tensile force in the reinforcement, the following equations can be derived for a certain surcharge.

$$\frac{F_2(x) - F_1(x)}{J_2 - J_1} = \alpha \quad J_{1,2} > 2000 \text{ kN/m} \tag{23}$$

$$\frac{F_2(x) - F_1(x)}{J_2 - J_1} = \beta \quad J_{1,2} < 2000 \text{ kN/m} \tag{24}$$

From Eqs. (22), (23) and (24):

$$\left( J_1 u_1(x) - J_2 u_2(x) \right) = \alpha (J_1 - J_2) x \quad J_{1,2} > 2000 \text{ kN/m} \tag{25}$$

$$\left( J_1 u_1(x) - J_2 u_2(x) \right) = \beta (J_1 - J_2) x \quad J_{1,2} < 2000 \text{ kN/m} \tag{26}$$

From Eqs. (20), (23) and (24):

$$\tau_1(x) = \tau_2(x) \tag{27}$$

From Eqs. (23), (24) and (21):

$$\left( J_1 \varepsilon_1(x) - J_2 \varepsilon_2(x) \right) = \alpha (J_1 - J_2) \quad J_{1,2} > 2000 \text{ kN/m} \tag{28}$$

$$\left( J_1 \varepsilon_1(x) - J_2 \varepsilon_2(x) \right) = \beta (J_1 - J_2) \quad J_{1,2} < 2000 \text{ kN/m} \tag{29}$$

Where:

- $F_1(x)$  and  $F_2(x)$  = tensile force in the reinforcement corresponding to the reinforcement stiffness  $J_1$  and  $J_2$ .
- $u_1(x)$  and  $u_2(x)$  = horizontal displacement in the reinforcement corresponding to the reinforcement stiffness  $J_1$  and  $J_2$ .
- $\tau_1(x)$  and  $\tau_2(x)$  = tangential shear stress in the reinforcement corresponding to the reinforcement stiffness  $J_1$  and  $J_2$ .
- $\varepsilon_1(x)$  and  $\varepsilon_2(x)$  = strain in the reinforcement corresponding to the reinforcement stiffness  $J_1$  and  $J_2$ .
- $x$  = distance from the center line of the embankment.

Eq. (25) indicates that for a certain surcharge, variation in the reinforcement stiffness has no effect on the tangential shear stress in the reinforcement.

**3.5. Surcharge rate**

Surcharge rate is an important factor in maintaining the short-term stability of embankments over soft foundation. Embankment stability is sensitive to surcharge rate, as is evident from the failure surcharge shown in Fig. 15. As shown in Fig. 15 the increase in reinforcement stiffness had more significant effect on the embankment failure surcharge for slower surcharge rates as the embankment failure surcharge was 214.6 kN/m<sup>2</sup> for surcharge rate = 18.18 kN/m<sup>2</sup>/month while that was 127 kN/m<sup>2</sup> for surcharge rate = 60.60kN/m<sup>2</sup>/month.

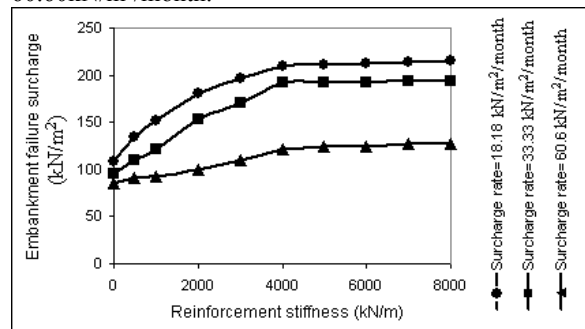


**Fig. 15.** Effect of Surcharge Rate on the Embankment Failure Surcharge.

#### 4. Conclusions

The response of an embankment on soft clay was investigated by a series of finite element analysis using Plaxis program. Conclusions that can be drawn from this study are summarized below.

- Geosynthetic reinforcement can substantially increase the stability and failure surcharge of embankments on soft foundations.
- There was a limit to the reinforcement stiffness which can be mobilized.

- Increasing the reinforcement stiffness does not contribute much to the reduction in vertical displacement compared to the horizontal displacement.
- The effect of stiff reinforcement was greater under slow surcharge rates than under fast surcharge rates.
- There were logical relationships between the tensile force, tangential shear stress, horizontal displacement and reinforcement stiffness for a certain surcharge of the embankment.

---

#### References

1. Bassett, R.H. and Yeo, K.C. 1998. The behavior of a reinforced trial embankment on soft shallow foundation. Proceeding of International Conference on Theory and Practice of Earth Reinforcement, Fukuoka, Japan, pp 371-376.
2. Fowler J., Schimelfenyg P. and Leshchinsky D. 1990. Fabric reinforced containment dike, New Bedford superfund site. Proceeding of the 4th International Conference on Geotextile, Geomembranes and Related Products, The Hague, Netherland, Vol. 1, pp 149-154.
3. Chai J.-C., Miura N. and Shen S.-L. 2002. Performance of embankments with and without reinforcement on soft subsoil. Canadian Geotechnical Journal 39, pp 838-848.
4. Row R.K. and Soderman K.L. 1985. Geotextile reinforcement of embankments on peat. Geotextiles and Geomembranes 2., pp 277-298.
5. Hinchberger S.D. and Rowe R.K. 1998. Modelling the rate-sensitive characteristic of the Gloucester foundation soil. Canadian Geotechnical Journal 35, pp 769-789.
6. Varadarajan A., Sharma K.G. and Aly M.A.A 1999. Finite element analysis of reinforced embankment foundation. International Journal for Numerical and Analysis in Geomechanics 23, pp 103-114.
7. Seed, R. B., Collin, J. G., and Mitchell, J. K. 1986. FEM analyses of compacted reinforced soil walls. "Proc., Second Symp. on Numerical Model in Geomechanics, Balkema, Rotterdam, The Netherlands, 533-562.
8. Schanz, T. Vermeer, P.A. 1998. On the Stiffness of Sand. Geotechnique, Special issue on Pre-failure Deformation Behaviour of Geomaterials, pp. 383 - 387.
9. Kondner, R.L. 1963. "Hyperbolic stress-strain response: Cohesive soils," Journal of the Soil Mechanics and Foundation Division, ASCE, proc. Paper 3429, 89(SM1), 115-143.
10. Duncan, J.M., Chang, C.-Y., 1970. Nonlinear Analysis of Stress and Strain in Soil. ASCE J. of the Soil Mech. and Found. Div. Vol. 96, pp. 1629-1653.
11. Rowe, R.K., 1992. "Reinforced Embankments on Soft Cohesive Deposits", Proceedings of the International Symposium on Application of Geosynthetics Technology, Jakarta, Indonesia, pp. 1-19.
12. Rowe, R.K., Granendran, C.T., Landva, A.O., and Valsangkar, A.J.,1995. "Construction and Performance of a Full Scale Geotextile Reinforced Test Embankment", Canadian Geotechnical Journal, Vol. 32, No.3, pp. 512-534.
13. Delmas, P., Queroy, D., Quaresma, M. and De Saint, A., 1992. "Failure of an Experimental Embankment: Guiche Geotextile, Geomembranes and Related Products", den Hoedt, Editor, Balkema Printers, Rotterdam.
14. Li, A. L. & Rowe, R. K., 2001. Influence of creep and stress-relaxation of geosynthetic reinforcement on embankment behaviour. Geosynthetics International, 8, No. 3, 233-270.